Bulletin of National University of Uzbekistan: Mathematics and Natural Sciences

Volume 3 | Issue 1 Article 11

4-9-2020

Photocatalytic performance of V_2O_5 nanoparticles incorporated TiO_2 nanotubes as a visible-light active photoelectrodefor water splitting

Ulugbek Shaislamov
National University of Uzbekistan, sulugbek@gmail.com

Kamil Mukimov
National University of Uzbekistan; Center for Development of Nanotechnology, Tashkent

Turgunali Akhmadjanov
National University of Uzbekistan

Bulletin of National University of Uzbekistan: Mathematics and Natural Sciences

PHOTOCATALYTIC PERFORMANCE OF V_2O_5 NANOPARTICLES INCORPORATED TIO_2 NANOTUBES AS A VISIBLE-LIGHT ACTIVE PHOTOELECTRODEFOR WATER SPLITTING

Shaislamov U.[1], Mukimov K.[1,2], Akhmadjanov T.[1]
[1]*National University of Uzbekistan, Tashkent, Uzbekistan*
[2]*Center for Development of Nanotechnology, Tashkent, Uzbekistan*
e-mail: sulugbek@gmail.com

Abstract

Herein we demonstrate brief investigation results of photoelectrochemical performance of TiO_2 nanotube (NT) based photoelectrode incorporated with V_2O_5 nanopaerticles (NP). Photoelectrodes were composed of TiO_2 NTs with a diameter of 100 nm and length of $8\mu m$,that were prepared by electrochemical anodization process at 35V in a formamade based electrolyte. The V_2O_5 nanoparticles were formed on the walls of the TiO_2 NTs by deep coating technique with an average size of ∼5-10 nm. The V_2O_5 NP incorporated TiO_2 NTs show superior light absorption properties in the visible light region up to ∼600 nm compared to the pristine TiO_2NTs. It was found that V_2O_5 NPs formed vanadium impurities within TiO_2 NTs which in its turn ceated acceptor levels of V^{3+} ions in the TiO_2 NTs located deep in the forbidden band gap and provided additional absorption properties of visible light. These impurity levels also provide fast recombination sites of electrons and holes formed by photon excitation.

Keywords:Photoelectrochemical cell, visible light, TiO_2 nanotubes, V_2O_5 nanoparticles.

Physics and Astronomy Classification Scheme: 85.60.Ha, 89.30.Cc, 61.46.+w, 73.40.Mr, 73.63.Rt.

1 Introduction

Energy consumption has been increasing more faster due to the of intensive grow of human population and industrialization. On the other hand, current power generation technologies relies on the fossil fuels, which reserves are limited. Continues use of fossil fuels arise many serious challenges, such as oil prices are forecast to continue to increase approximately $ 125–200 per barrel by the year 2035, which was approximately $ 80 in 2008. Another big problem continues use of fossil fuels is the environmental pollution, by emission of harmful CO $_2$ gases [1, 2]. Therefore, development of renewable energy resources is very important. The renewable energy has great potential to be exploited for extensive use in the near future. The technical potential of renewable energy sources are 30 times more than the current global primary energy use, and several times higher than the predicted energy use 2100 (4x10 ^{20}J). The theoretical potential means the amount of energy theoretically available energy purposes, such as solar energy, the amount of incoming radiation at the surface of the

earth. The technical potential of the renewable energy resources clearly indicates that the renewable energy has great margin to be used as the primary energy for human activity. Solar energy has the highest fraction among the alternative energy resources, thus is considered to be the most promising resource. However, solar energy need to be effectively converted in to accessible energy sources, such as heat, chemical energy, electrical, etc. The most widely practical using example of energy conversion system is photovoltaic cells, which converts solar energy to electrical one with high efficiency. However, present solar cells are built using expensive single crystalline Si, which cannot provide all energy need consumed by human. Dye sensitized solar cells (DSSC) is one of the most advanced device for solar energy conversion with high efficiency. The device is able to convert the solar energy in to electrical one with efficient of 11% and can be simply fabricates by utilizing low cost materials. Furthermore, hydrogen is forecasted to be the main energy source in the future, because it is environmentally clean. However current technologies of hydrogen generation is dependent on fossil fuels and it is not advantageous in terms of environmental and economical point of view[3, 4]. Decomposition of water in to H_2 and O_2 using solar energy is an alternative technology to produce H_2 without damage to environment, and is recently most intensively studied field of research. [5]. In the original work by the A. Fujishima, the PEC cells consisted of n-type TiO_2 working electrode and Pt counter electrode. When semiconductor is illuminated with photons with energies larger than that of a bandgap, electrons and holes are generated in the conduction and valence bands, respectively. The photogenerated electrons and holes cause re/dox reactions similarly to electrolysis. Water molecules are reduced by the electrons to form H_2 and are oxidized by the holes to form O_2 for overall water splitting. Width of the bandgap and the location of the levels of the conduction and valence bands are one of the essential points in the semiconductor photocatalyst materials. The bottom level of the conduction band has to be more negative than the redox potential of H^+/H_2 (0 V vs. NHE), while the top level of the valence band be more positive than the red/ox potential of O_2/H_2O (1.23 V). Therefore, the theoretical minimum bandgap for water splitting is 1.23 eV that corresponds to light of about 1100 nm. There are several factors that affect the efficiency of the photocatalyst material. Some of the important factors influencing the water splitting process are the crystal structure, crystallinity and particle size of the photocatalyst. Materials with higher crystalline quality have lower degree of defects. The defects in the photocatalyst material act as trapping and recombination centers between photogenerated electrons and holes, resulting in a decrease in the photocatalytic activity. Recombination rate can be decreasing by reducing the particle size of the photocatalyst. Because in small size particles the photoelectrons migrate shorter distance to the reaction sites, thus chance of recombination is lowers. Further, in order to improve the efficiency of the process, it is necessary to develop photo-electrolysis electrodes that can effectively harvest visible light consisting of 45% in sunlight spectrum. So far, there have been many efforts to address this issue, such as band gap engineering, inhibitive recombination of photo-generated carriers, Z-scheme, tandem cell and control of active surface sites for redox reactions [6-10]. The primary approaches to making a wide-gap metal oxide

sensitive to visible light can be classified as follows: (1) Doping with transition-metal ions having a d_n ($0 < n < 10$) electronic configuration, (2) valence band control using an anion's p orbitals or the s orbitals of p-block metal ions, (3) spectral sensitization. In the Z-scheme approach, two photocatalyst materials with different band positions can be utilized. One photocatalyst for water oxidation and the other is for water reduction, thus it is possible to overcome the need to design a single, ideally suitable material. Further, the effective operation of the two materials could be controlled by a suitable redox shuttle media. In the tandem cell structure, a single, suitable photoelectrode is coupled with a solar cell that will provide necessary bias to facilitate the water splitting reaction. Often, solar cells that are used in the tandem cells are based on the transparent substrate, such as dye sensitized solar cell, to promote effective integration of the whole system. Semiconductors with the band gap feasible to absorb the visible light should have simultaneously suitable band levels relative to water reduction H^+/H_2 and water oxidation O_2/H_2O potentials to generate efficient hydrogen through photo-electrolysis of water. For example, conduction band position of WO_3 electrodes located lower than that of water reduction potential (H^+/H_2) and thus do not properly function for H_2 evolution. In case of some other materials, having an ideal position of water redox potentials, such as CdS (CdS also have a low band gap of 2.4 eV to absorb visible light), this materials would decompose under photoelectrochemical conditions due to photocorrosion issue. Among other materials, TiO_2 have relatively suitable conduction and valence band levels for the water redox reaction and also possess chemical stability. However, due to its large band gap (3.0∼3.1 eV) it absorbs only UV light, which corresponds to 2-3% of the sunlight spectrum. There have been many efforts to enhance the absorption of the visible light in TiO_2. For example, control of band gap through doping with N, C, and S ions in TiO_2 showed improvement of the visible light efficiency [11-16]. Another approach to enhance the absorption of the visible light in TiO_2 is to modify the absorption spectrum of TiO_2 by using semiconductors with different structure of energy band. Sufficient surface properties and area for the redox reaction of H_2O are also very important even though band structures of electrodes are suitable. Activated surface for the redox reactions should be large enough to restrain from recombination of electrons and holes.

In this work, we report a systematic investigation of the V_2O_5 nanoparticle incorporated TiO_2 NT photoelectrode to address the issues of improving the efficiency of solar-hydrogen evolution under visible light. Visible light absorption properties of the TiO_2 NT based photoelectrode was achieved by sensitization with the V_2O_5 NPs that form distinct V_2O_5 nanoparticles on the surface of TiO_2NTs. It is shown that photo-electrolysis efficiency in visible light of the TiO_2 NTs sensitized with the NPs was improved significantly up to ∼10 times.

2 Experimental methods

2.1 Preparation of Photoelectrodes

TiO_2 nanotubes arrays were fabricated by electrochemical anodization of Ti foils with thickness of 0.1mm and 99.6% purity (Alfa Aesar). First, Ti plates were cleaned by sonification in TCE, acetone, and methanol and dried under N_2 stream. As prepared Ti foils were anodized in formamide based electrolyte at 35 V for 3hr at room temperature. A platinum foil was used as the counter electrode. Anodization techniques using organic electrolytes such as dimethyl sulfoxide (DMSO), formamide (FA), ethylene glycol, and *N*-methylformamide (NMF) are feasible for fabricating long TiO_2 nanotube arrays as described in [17-19]. Amorphous TiO_2 NTs formed by the anodization processes were annealed for crystallization at 550^oC in air for 4hr. Formation of the V_2O_5 NPs on the crystallized TiO_2 NTs were achieved by dip coating technique in to a solution containing a vanadium source. The crystallized TiO_2 NTs were dipped into the liquid solutions for 30 min and baked at 100^oC for 1hr. Vanadium oxides absorbed on surface of the TiO_2 NTs were crystallized at 400^oC for 1hr in air ambient.

2.2 Micro structural and Optical Characterization

Observation of nano-structured samples was performed using SEM (JSM-6500F) and TEM (JEM 2100). Crystalline state of TiO_2 NTs and V_2O_5NPs was confirmed by an x-ray diffractometer (XRD-SWXD). The CuK radiation source was operated at 40 kV and 40 mA. The 2 θ scan data were collected using a scintillation detector at 0.01° intervals over the range 20° to 80° and a scan rate of 3 °/sec.

2.3 Electrochemical Characterization

Electrochemical measurements were performed using a three electrodes system (AMT VERSASTAT3) consisting of a Pt wire counter electrode and a saturated Ag/AgCl reference electrode. The potential was swept linearly at a scan rate of 50 mV/s. Water photoelectrolysis tests for 1 cm^2 working electrodes, illuminated using a 1 KW xenon lamp from which infrared wavelengths were filtered by water, carried out in a 1M KOH electrolyte. The measured light irradiance was 100 mW/cm^2. For visible-light illumination, wavelength below 420 nm was cut off by an optical filter.

2.4 Results discussion

In the past decade, TiO_2 nanotube arrays fabricated by electrochemical anodization of titanium (Ti) metal have attracted great attention for their high specific surface area, vertically oriented nanostructure, high chemical stability and simple preparation. It is worth noting that, unlike powdered nanostructured TiO_2, these TiO_2 nanotube arrays can be employed directly as an electrode in some devices since the nanotube arrays are directly attached to the underlying Ti metal. Interestingly, the TiO_2 nanotube arrays

produced in this way are generally amorphous and it was found that, for amorphous nanotubes, water-induced crystallization with a concomitant change in morphology can occur when exposed to water. In fact, the early Ti was anodized in an aqueous solution of HF to get TNTs. However, the corrosiveness of HF is too strong, and the prepared nanotubes have poor regularity, so researchers began to get nanotubes by the anodization in fluoride-containing electrolytes with organic solvents. In general, self-ordered and close-packed TNTs can be obtained by using conventional ethylene glycol (EG) electrolytes under optimized conditions. There is no or very narrow gap between these nanotubes. However, spaced nanotubes can also be achieved in certain electrolyte containing special organic solvents. It has been demonstrated fabricationof spaced nanotubes in diethylene glycol (DEG) based electrolytes. Further, partially spaced nanotubes can also be obtained in glycerol (GI) electrolytes. The nature of electrolyte used for the development of NTs strongly influences the formation of the graded structure. It was well recognized that under the same conditions, different electrolytes may produce different electric field intensities. It was also well known that in the initial stage of anodization, the higher electric field intensity can induce bigger breakdown sites which finally result in wider diameter of NTs. Additionally, the chemical dissolution rate of oxide layer is also discrepant in different electrolytes. In other words, one can obtain different titanium oxide structures such as a flat compact oxide, a disordered porous layer, a highly self-organized porous layer, and/or finally a highly self-organized nanotubular layer by controlling the electrochemical anodization parameters of Ti .

The NTs can be synthesized by anodization using various fluoride-containing electrolytes like NH_4F/CH_3COOH, H_2SO_4/HF, Na_2HPO_4/NaF, etc. The nanotube diameter is remarkably affected by the electrolytes used. Generally, two different types of electrolytes such as organic (or neutral) and aqueous electrolytes have been used for the synthesis of NTs. When the anodization takes place in an acidic condition of pH, in other words, high water content is called aqueous electrolytes. An organic (or neutral) electrolyte has a small amount of oxygen/water content in comparison to an aqueous electrolyte.

In the organic electrolyte like $(NH_4)H_2PO_4/NH_4F$ and $(NH_4)_2SO_4/NH_4F$, longer nanotube length and better self-organized TNT layers were obtained. These self-organized porous structures have large potential and commercial applications in view of several interesting properties. Neutral and viscous electrolytes allow better control in the anodic conditions and creating two different environments along the tube, one inert at the top of it and other chemically reactive at the bottom. Thus, the inhibition of the oxide dissolution at the top side of the nanotube allows the formation of longer NTs. Much higher current densities are observed in the aqueous electrolytes than in the organic electrolyte, which is attributed to higher diffusibility and concentration of ions in aqueous electrolytes. However, smooth curves were obtained at all voltages in the glycerol (organic) electrolytes, whereas current fluctuations were observed in aqueous electrolyte which is due to the high rate of chemical dissolution and the oxidation of Ti.

TiO_2 nanotubes (NTs) used as a nano-structured main frame for V_2O_5nano-

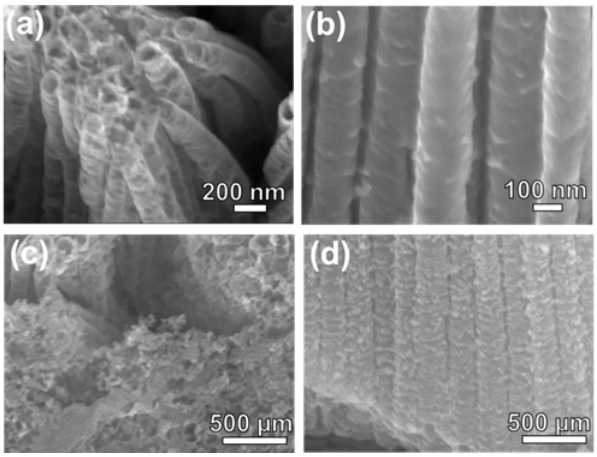

Figure 1: FESEM images of the TiO_2/V_2O_5 NTs. (a) Top and (b) cross-sectional view of the pristine TiO_2 NTs. FESEM Top view (c) and (d) cross-sectional view of the TiO_2 NTs coated with V_2O_5 NPs.

particles (NPs) were fabricated by the anodization of Ti plate using formamide-based electrolytes, as shown in Figure 1(a) and (b) for top and cross-sectional views, respectively. The diameter and the length of the TiO_2 NTs were 100 nm and $\sim 8\mu$m, respectively. It can be seen that TiO_2 NTs have distinct tubular structure with open ends at the top (see Fig. 1(a)). Nanotubes grow almost perpendicular to the substrate which can be seen from the cross-sectional view, shown in the Fig. 1(b). As prepared amorphous TiO_2 NTs, fabricated by the anodization, were crystallized at 550^oC in air for 4hr, and then the NTs were dipped into liquid source including vanadium-oxide ligands for 30 min and dried at 100^oC for 1hr. Then the samples were annealed at 400^oC for 1hr to crystallize V_2O_5 NPs absorbed on the wall of TiO_2 NTs. The SEM images of the V_2O_5 sensitized NTs are shown in the Figure 1(c) and (d) which shows the V_2O_5 NPs in the range of 5-10 nm that almost uniformly covered the TiO_2 NTs. As showed in the Figure 1(c), the surface of TiO_2 NT arrays even after annealing for the crystallization of V_2O_5 NPs was still cleaned without any coverage of V_2O_5 NPs.

It is important the surface to be kept opened for photoelectrolysis tests under light irradiance. Otherwise, the area for the light absorbance will be diminished and the redox reactions on the surface of the TiO_2 NTs also decreased under light illumination.

The XRD measurements confirmed that the NPs on the TiO_2 NTs were in the V_2O_5 phase with a hexagonal structure. The XRD peaks of the NPs on the TiO_2 NTs were also compared with those of the TiO_2 NT arrays without the NTs, as shown in Fig. 2. The XRD peaks of the rutile and the anatase phases were observed in both the samples of TiO_2 NTs with and without NPs. The XRD analysis confirmed that the phase structures of the TiO_2 NTs did not change even after the thermal treatment for crystallization of the NPs.

Transmission electron microscope (TEM) analysis of the TiO_2/V_2O_5 samples revealed that the TiO_2 NTs have distinct tubular structure with a narrow diameter

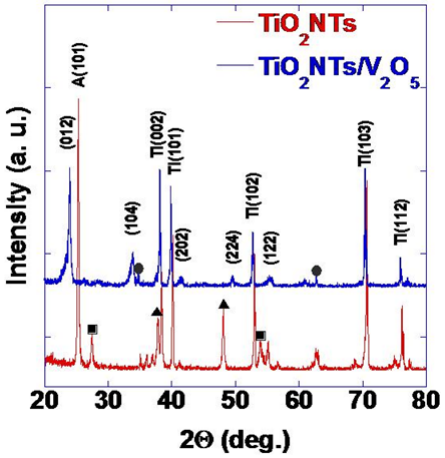

Figure 2: XRD patterns of theTiO_2 NTs and V_2O_5coated TiO_2 NTs.

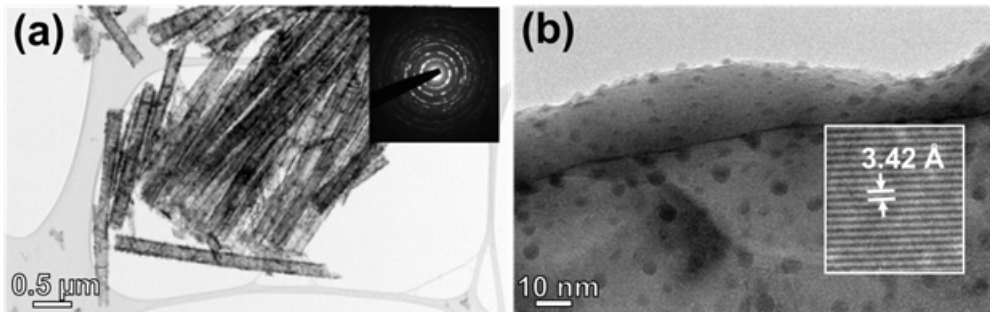

Figure 3: TEM images of TiO_2/V_2O_5 NTs. (a) Low-magnification bright-field and (b) high magnification bright-field images of TiO_2/V_2O_5 NTs. Inset of the (a) shows electron diffraction image.

distribution. Their walls are rather rough and have polycrystalline structure as can be seen from the diffraction pattern shown in the inset of the Fig. 3. Figure 3(b) shows high-magnification TEM images of the TiO_2/V_2O_5 where V_2O_5 NP are clearly seen. The V_2O_5 NP is uniformly distributed through the TiO_2 NT with a size of 5-6 nm.

Photocurrent measurements for TiO_2 NTs with and without V_2O_5 NPs were carried out to examine the photoelectrochemical properties of the photoelectrodes under chopped illumination of white and visible lights as shown in Fig. 4(a) and (b), respectively. The photocurrent response of samples for a constant irradiation normally includes both the pure photocurrent from the light irradiation and the current caused by the applied bias used for the measurements. Therefore, the illuminating light was chopped during photocurrent measurement to reveal the real photocurrent contributing to the electrolysis process.

The heights in the stepped photocurrents in Figs. 4(a) and (b) formed by chopping the light illumination. The photocurrent height was re-plotted in the Figs. 4(c) and (d) for the white and visible light measurements, respectively. For white irradi-

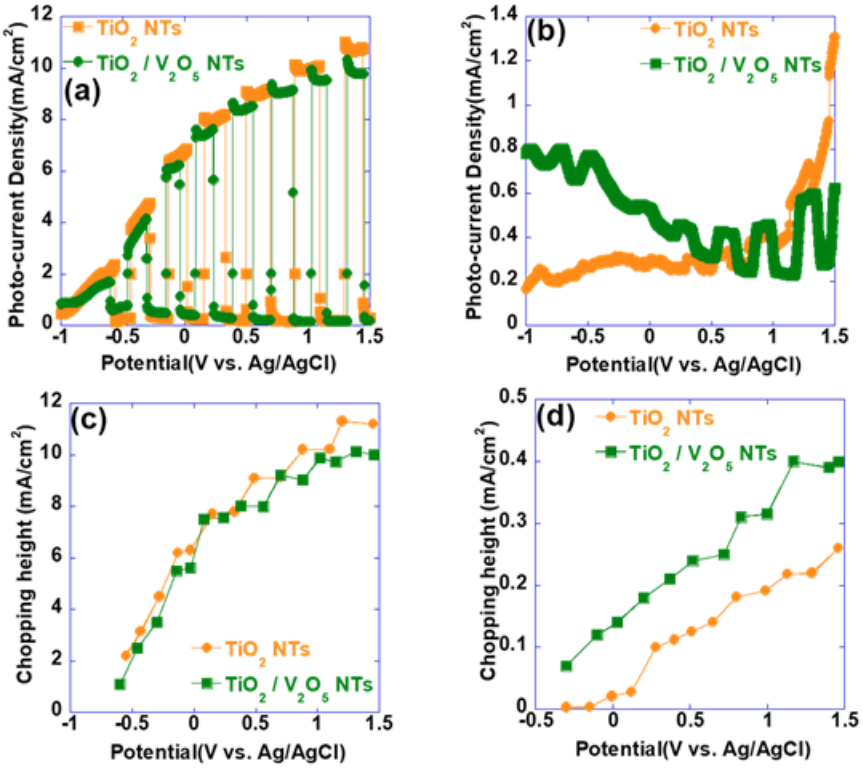

Figure 4: Photocurrent density measurements under (a) white light and (b) only visible light for TiO_2 NTs and TiO_2/V_2O_5 NTs. Chopping height of the photocurrent density under (c) white light and (d) visible light for TiO_2 NTs and TiO_2/V_2O_5 NTs.

ation, the photocurrent height of the TiO_2 NTs is around 2 times larger than that of TiO_2 NTs/V_2O_5 NPs. However, the photocurrent under visible light increases significantly with increasing applied bias and saturates at a bias of about -0.1V, while the TiO_2 NTs show almost insignificant responses under visible light. The photoconversion efficiency $\eta(\%)$ ([total power output- electrical power output]/light power input) [13], the ratio of converted chemical energy to input photon energy, were calculated from the measured photocurrent heights of Fig. 4(c) and (d) and are presented in Fig. 5(a) and (b) for white and visible light measurements, respectively. The photoconversion efficiency under white light for TiO_2 NTs is $\sim$17%, which is higher than that of TiO_2 NTs/V_2O_5 NPs, ($\sim$7%) as shown in Fig. 5(b). In the measurements under visible light, an efficiency of $\sim$1.2% was observed for the TiO_2 NTs/V_2O_5 NPs photoelectrode, however the pristine TiO_2 NTs' response was negligible (Fig. 5(b)).

Monochromatic measurements were performed to calculate incident photon to current efficiency (IPCE) at wavelengths ranging from 350 to 700 nm at a potential of +0.3 V versus Ag/AgCl as shown in the Fig. 6(a). In these measurements, the TiO_2 NTs/V_2O_5 NPs samples showed responses to visible light up to wavelengths of $\sim$500 nm. The band gap energy of those samples were determined directly from the intercept with the x-axis in a plot of $(\eta(\lambda)h\nu)^{1/2}$ versus $h\nu$ in Fig. 6(b) by using the

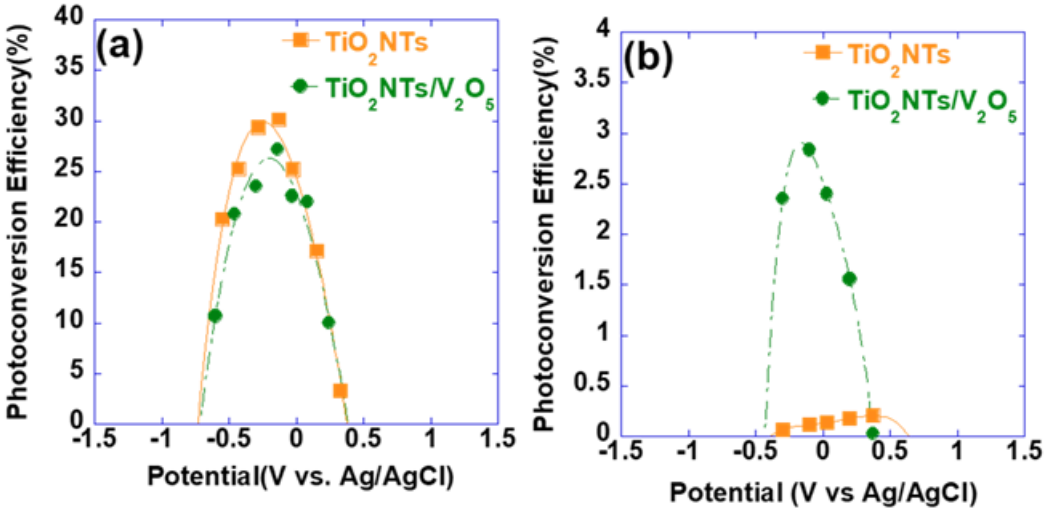

Figure 5: Photoconversion efficiency measured under (a) white (UV and visible) light and (b) visible light illuminations for TiO_2 NTs and TiO_2/V_2O_5 composite NTs.

following equation:

$$\eta(\lambda)h\nu = A(h\nu - E_g)^n, \tag{1}$$

where $\eta(\lambda)$ is the quantum efficiency ($\eta(\lambda)$=$j_p(\lambda)/e_oI_o(\lambda)$,the ratio of the number of charge carriers collected to the number of photons of a given energy illuminating the sample), A is a constant, and n is 2 for indirect transitions [20-25]. From the intercept with the x-axis, a band gap of 3.0 eV samples was measured for TiO_2 NTs. The band-gap energy of the TiO_2 NTs/V_2O_5 NP photoelectrode was measured as 2.7 eV, as shown in Fig. 6(b), which is indication that the photoelectrode is active in the visible spectrum o the illumination.

Conclusion

In conclusion, the photocatalytic properties of the V_2O_5 NP incorporated TiO_2 NT photoelectrode were systematically investigated and compare with those of pristine TiO_2NTs. The TiO_2 NTs were sensitized with low band NP in order to address the issues of improving the efficiency of hydrogen evolution under visible light. The V_2O_5NPs with an average size of 5-10 nm were formed on the walls of TiO_2 NTs by deep coating method followed by a heat treatment process. The photo-electrolysis efficiency of the TiO_2/V_2O_5NTs under visible light increased significantly compare to the pristine TiO_2 NTs without NPs. An examination of the photoresponse of V_2O_5 NPs on TiO_2 NTs indicated that the V_2O_5 NPs showed superior photoresponse for visible light and that the interfaces between V_2O_5 NPs and TiO_2 NTs acted as fast recombination sites in the TiO_2 NTs during irradiation with white light.

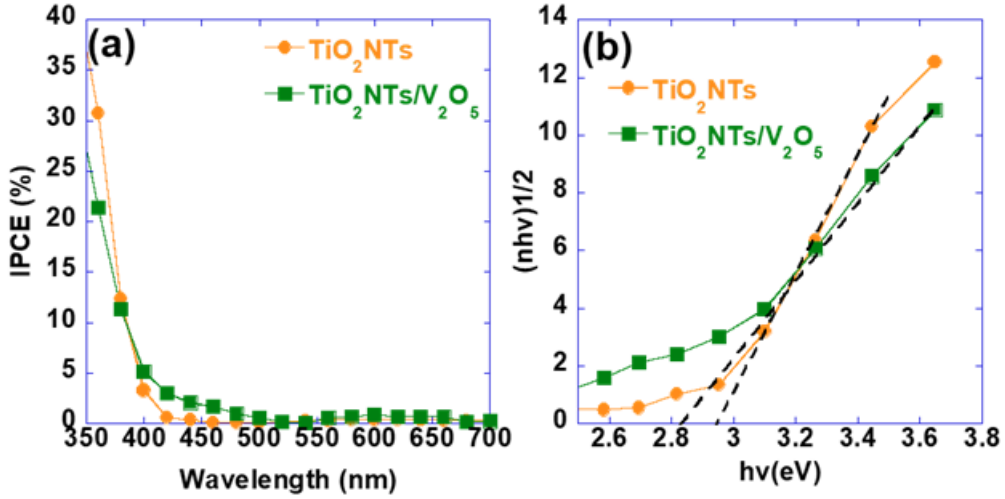

Figure 6: (a)Incident Photon to Current Efficiency (IPCE) and (b) quantum efficiency of the pristine TiO_2 NTs and TiO_2 NTs/V_2O_5 NPs photoelectrodes.

References

[1] Woodhousea M., Parkinson B. A. Combinatorial approaches for the identification and optimization of oxide semiconductors for efficient solar photoelectrolysis. Chem. Soc. Rev. **38**, 197-210(2009).

[2] Kudo A., Miseki Y. Heterogeneous photocatalyst materials for water splitting. Chem. Soc. Rev. **38**, 253-278 (2009).

[3] Wang Z., Li C., Domen K. Recent developments in heterogeneous photocatalysts for solar-driven overall water splitting. *Chem. Soc. Rev.*, **48**, 2109-2125 (2019).

[4] Miseki Y., Sayama K. Photocatalytic water splitting employing a $[Fe(CN)_6]^{-3/-4}$ redox mediator under visible light. Catal. Sci. Technol., 9, 2019-2024, (2019).

[5] Fujishima A., Honda K. Electrochemical Photolysis of Water at a Semiconductor Electrode. Nature **238**, 37-38 (1972).

[6] Darwent J.R., Mills A. Photo-oxidation of water sensitized by WO_3 powder. J. Chem. Soc., Faraday Trans. **78,** 359-367 (1982).

[7] Pleskov Y.V., Gurevich Y.Y. Semiconductor Photoelectrochemistry, Plenum, New York (1986).

[8] Nisar J., Wang B., Araujo C. M. A. Ferreira da Silvac, T. W. Kang, R. Ahuja, Band gap engineering by anion doping in the photocatalyst $BiTaO_4$: First principle calculations. Int. J. Hyd. Ener., **37**,3014-3018, (2012)

[9] Samsudin E.M., Hamid S.B. Effect of band gap engineering in anionic-doped TiO_2 photocatalyst. Appl. Sur. Sci. **391**, 326-336 (2017).

[10] Vitiello R.P., Macak J.M. A. Ghicov, H. Tsuchiya, L.F.P. Dick, P. Schmuki, N-Doping of anodic TiO_2 nanotubes using heat treatment in ammonia. Electrochem. Commu. **8**, 544-548 (2006).

[11] Asahi R., Morikawa T., Ohwaki T., Aoki K., Taga Y. Visible-Light Photocatalysis in Nitrogen-Doped Titanium Oxides, Science **293**, 269-271 (2001).

[12] Kosowska B., Mozia S., Morawski A., Grznil B., Janus M., Kalucki K. The preparation of TiO_2–nitrogen doped by calcination of $TiO_2 \cdot xH_2O$ under ammonia atmosphere for visible light photocatalysis. Sol. Energy Mater. Cells **88**, 269-280 (2005).

[13] Park Y., Kim W., Park H., Tachikawa T., Majima T., Choi W. Carbon-doped TiO_2 photocatalyst synthesized without using an external carbon precursor and the visible light activity. Appl. Catal B: Environ. **91**, 355-364 (2009).

[14] Hariharan D., Jegath A.Ch., Mayandi J., Nehrua L.C. Visible light active photocatalyst: hydrothermal green synthesized TiO_2 NPs for degradation of picric acid. Mater. Lett., 222, 45-49 (2018).

[15] Shaislamov U., Lee H.J. Facile synthesis of Ag/ZnO metal–semiconductor hierarchical photocatalyst nanostructures via the galvanic-potential-enhanced hydrothermal method. CrystEngComm, **20**, 7492-7501 (2018).

[16] Shaislamov U., Krishnamoorthy K., Kim S.J., Abidov A., Allabergenov B., Kim S., Choi S., Suresh R., Ahmed W.M., Lee H.J. Highly stable hierarchical p-CuO/ZnO nanorod/nanobranch photoelectrode for efficient solar energy conversion. Int. J. Hyd. Ener., **41**2253-2262 (2016).

[17] Ruan C., Paulose M., Varghese O.K., Mor G.K., Grimes C.A. Fabrication of highly ordered TiO_2 nanotube arrays using an organic electrolyte. J. Phys. Chem. B**109,**15754-15759 (2005).

[18] Shankar K., Bandara J., Paulose M., Wietasch H., Varghese O.K., Mor G.K., LaTempa T.J., Thelakkat M., Grimes C.A. Highly efficient solar cells using TiO_2 nanotube arrays sensitized with a donor-antenna dye. Nano Lett.**8**,1654-1659 (2008).

[19] Mor G.K., Varghese O.K., Paulose M., Shankar K., Grimes C.A. A review on highly ordered, vertically oriented TiO_2 nanotube arrays: Fabrication, material properties, and solar energy applications.Sol. Energy Mater. Cells **90**, 2011-2075 (2006).

[20] Khan S.U.M., Akikusha J. Photoelectrochemical splitting of water at nanocrystalline n-Fe_2O_3 thin-film electrodes. J. Phys. Chem. B**103**, 7184-7189 (1999).

[21] Shahed U.M., Sultana K.T. Photoresponse of n-TiO_2 thin film and nanowire electrodes. Sol. Energy Mater. Cells **76 2**, 211-221 (2003).

[22] Akikusa J., Khan S.U.M., Photoelectrolysis of water to hydrogen in p-SiC/Pt and p-SiC/ n-TiO_2 cells. Int. J. Hydrogen Energy**27**, 863-870 (2002).

[23] Pankove J.I. Optical Process in Semiconductor, Chapter 3, Dover, New York (1971).

[24] Kato H., Kudo A., Visible-light-response and photocatalytic activities of TiO_2 and $SrTiO_3$ photocatalysts codoped with antimony and chromium J. Phys. Chem. B **106**, 5029-5034 (2002).

[25] Ikeda T., Nomoto T., Eda K., Mizutani Y., Kato H., Kudo A., Onishi H. Photoinduced dynamics of TiO_2 doped with Cr and Sb. J. Phys. Chem. C **112**, 1167-1173 (2008).